Title
3D Monte Carlo model of optical transport in laser-irradiated cutaneous vascular malformations

ISBN
9780819476524

Authors
Majaron, Boris
Milanič, Matija
Jia, Wangcun
et al.

Publication Date
2010-06-25

DOI
10.1117/12.871058

3D Monte Carlo model of optical transport in laser-irradiated cutaneous vascular malformations

Boris Majaron*[a,b], Matija Milanič[a], Wangcun Jia[c], J. Stuart Nelson[c]
[a]Jožef Stefan Institute, Jamova 39, SI-1000 Ljubljana, Slovenia
[b]Faculty of Mathematics and Physics, University of Ljubljana, Slovenia
[c]Beckman Laser Institute, University of California, Irvine, CA 92612, USA

ABSTRACT

We have developed a three-dimensional Monte Carlo (MC) model of optical transport in skin and applied it to analysis of port wine stain treatment with sequential laser irradiation and intermittent cryogen spray cooling. Our MC model extends the approaches of the popular multi-layer model by Wang *et al*.[1] to three dimensions, thus allowing treatment of skin inclusions with more complex geometries and arbitrary irradiation patterns. To overcome the obvious drawbacks of either "escape" or "mirror" boundary conditions at the lateral boundaries of the finely discretized volume of interest (VOI), photons exiting the VOI are propagated in laterally infinite tissue layers with appropriate optical properties, until they loose all their energy, escape into the air, or return to the VOI, but the energy deposition outside of the VOI is not computed and recorded. After discussing the selection of tissue parameters, we apply the model to analysis of blood photocoagulation and collateral thermal damage in treatment of port wine stain (PWS) lesions with sequential laser irradiation and intermittent cryogen spray cooling.

Keywords: Monte Carlo; three dimensions; boundary condition: cryogen spray cooling; multiple cryogen spurts; multiple laser pulses; vascular lesion; port wine stain;

1. INTRODUCTION

Cutaneous vascular lesions are nowadays treated with short-pulse orange, yellow or light green lasers, according to the principle of selective photothermolysis.[2] Introduction of precooling of skin surface by cryogen sprays (CS)[3] has offered significant protection against permanent thermal damage, occurring as a result of nonselective absorption of laser light in epidermal melanin. This allows safe application of larger radiant exposures, leading directly to improved treatment efficacy.

Nevertheless, the response of individual port wine stain (PWS) lesions remains highly variable, with many patients' PWS fading only minimally.[4,5] One plausible reason for poor treatment outcome is optical screening in large PWS vessels, due to limited penetration depth of the strongly absorbed laser light.[6] This effect prevents uniform coagulation of the entire vessel lumen with single short laser pulses, thus allowing the pathological vessels to recover from such partial damage.[7] In addition, the risk of epidermal thermal damage often limits the maximal safe radiant exposure to levels inadequate for permanent PWS vessel coagulation, especially in patients with darker skin.

One possible approach to these problems is to divide the radiant exposure into a sequence of multiple laser pulses (MLP) while controlling the epidermal temperature with multiple cryogen spurts (MCS) applied before each laser pulse. Our recent numerical and animal model study showed that such MCS-MLP treatment can provide photocoagulation of much larger blood vessels as compared to the customary approach (i.e., SCS-SLP) without increasing the risk of adverse side effects.[8] This may be a viable approach to improved therapeutic outcome for patients with darker skin and/or PWS featuring blood vessels of larger caliber.

In order to study the effects of laser pulse number (n) and repetition rate (f) on coagulation of ectatic PWS blood vessels and on epidermal thermal damage, we have developed a three dimensional numerical model of optical transport in PWS lesion, complemented by modeling of thermal transport and tissue coagulation kinetics.

*boris.majaron@ijs.si; phone +386 1 477-3208; fax +386 1 423-5400; complex.ijs.si

Laser Applications in Life Sciences, edited by Matti Kinnunen, Risto Myllylä, Proc. of SPIE Vol. 7376, 737608 · © 2010 SPIE · CCC code: 0277-786X/10/$18 · doi: 10.1117/12.871058

Our MC model extends the approach of the popular multi-layer model by Wang *et al.*[1] to three dimensions, thus allowing treatment of skin inclusions with more complex geometries and arbitrary irradiation patterns. A special care is devoted to implementation of realistic boundary conditions. In earlier documented 3D MC models, either the photon escape or reflective side boundaries were applied. Clearly, none of these approaches is appropriate for treatment of relatively small volume inside the human skin with arbitrary inclusions and irradiated with a spatially confined laser beam. To overcome this problem, photons exiting the finely discretized volume of interest (VOI) are propagated in laterally infinite tissue layers with appropriate optical properties, until they loose all their energy, escape into the air, or return to the VOI, but the energy deposition outside of the VOI is not computed and recorded. The same principle is applied also at the bottom of the VOI.

After discussing the selection of tissue parameters, we present some results from our analysis of blood photocoagulation and collateral thermal damage in port wine stain (PWS) treatment with sequential laser irradiation and intermittent cryogen spray cooling using a Nd:YAG/KTP laser (wavelength: $\lambda = 532$ nm) with 1 ms long individual pulses.

2. METHODOLOGY

2.1 Optical transport model

Simulation of light transport in PWS skin is based on the weighted-photon Monte Carlo (MC) technique.[1] In this scheme, a large number of energy packets ("photons") propagate through the tissue and deposit a fraction of their energy into specific volume elements, according to the local tissue absorption properties. Stochastic relations are used to simulate each photon's random trajectory, according to physical laws of light scattering, reflection, and refraction. These relations incorporate optical properties, specifically, absorption coefficient (μ_a), scattering coefficient (μ_s), anisotropy (g), and index of refraction (n) of the involved tissues. With increasing number of simulated photons and ever finer spatial discretization of the treated volume, the obtained energy deposition matrix ideally converges toward the actual distribution of absorbed light energy.

Our code extends the popular multi-layer MC model (a.k.a. MCML)[1] to three dimensions, thus allowing treatment of skin inclusions of arbitrary shape and optical properties. A special care was devoted to implementation of realistic boundary conditions. In earlier documented 3D MC models, either reflective ("mirror") side boundaries or photon escape boundaries were applied. The first approach is accurate only for infinitely wide irradiation and periodically distributed absorbing objects, while the second is suitable only for treatment of whole organs surrounded by air. Clearly, neither approach is appropriate for treatment of relatively small volume inside the human skin with arbitrary inclusions and irradiated with a spatially confined laser beam.

To overcome this problem, we continue by propagation of photons exiting the finely discretized volume of interest (VOI) in laterally infinite tissue layers until they return to the VOI, escape into the air, or loose all their energy. To reduce the computational burden and memory requirements, however, the energy deposition outside of the VOI is not computed and recorded. The same principle is applied also at the bottom boundary of the VOI.

In the presented example, the VOI dimensions are 1 mm × 1 mm in the plane parallel to the skin surface (coordinates x and y) and 2 mm in depth (z). The spatial discretization step is 2 μm × 2 μm in the plane perpendicular to the vessel axis, and 20 μm along the vessel axis.

The MC code is implemented in Visual C++ programming language (Visual studio 2008, Microsoft, Redmond, WA). Utilization of multiple threads helps speed up the computation. The average computation time for each MC simulation run with 10^7 simulated photons amounts to 9 minutes on a personal computer with Core 2 Duo processor P8600 (Intel, Santa Clara, CA) and 4 GB of 800 MHz RAM (DDR2).

2.2 PWS model geometry and optical parameters

Our skin model consists of laterally infinite layers, representing the epidermis (thickness: 60 μm), dermis (1.5 mm), and semi-infinite adipose layer underneath. In the dermis, we consider a single horizontal blood vessel with diameter of 150 μm and its axis 400 μm below the skin surface (Figure 1).

Melanin is assumed to be homogeneously distributed in the epidermis, with the epidermal absorption coefficient set to $\mu_{a,epi} = 2.0$ mm^{-1}. Based on analysis of diffused reflectance spectra by Svaasand *et al.*[9] and the commonly used

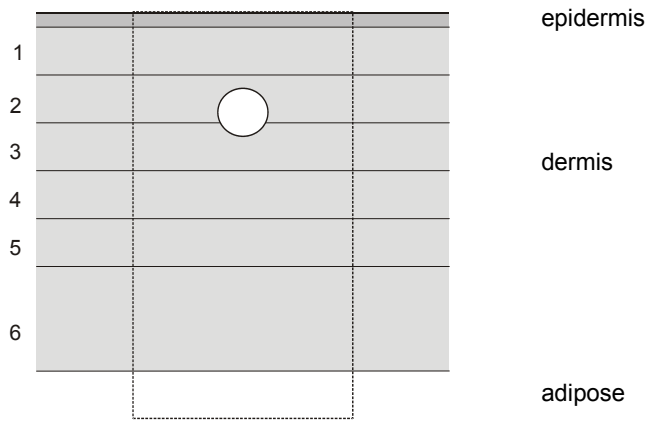

Figure 1: Cross-sectional view of the 3D model geometry, featuring the epidermal layer (*dark gray*), six dermal layers with different absorption properties (*gray*), a horizontal PWS blood vessel (*white*) located at depth of 400 μm, and the adipose layer underneath. Dashed lines mark the borders of the finely disretized volume of interest (VOI).

wavelength dependence relations by Jacques,[10] this corresponds to moderately pigmented Middle Eastern or Asian skin (effective fractional volume of melanin: $f_{\mathrm{mel}} = 3.5\%$).

In accordance with PWS histology data,[11] the dermis is divided into five 200 μm thick layers and one layer with thicknesses of 500 μm. The corresponding absorption coefficients $\mu_{\mathrm{a},i}$ are calculated by taking into account the reported mean blood vessel sizes and blood fractions (Table 1) as:

$$\mu_{\mathrm{a},i} = f_i\, C_i\, \mu_{\mathrm{a,bld}} + \left(1 - f_i\right) \mu_{\mathrm{a,der}} \tag{1}$$

Here, $\mu_{\mathrm{a,der}}$ is the absorption coefficient of bloodless dermis (0.053 mm^{-1}),[12] f_i is the fractional volume of blood in the i-th dermal layer, and C_i is the correction factor accounting for optical screening in PWS blood vessel of the corresponding radius r_i:[13,14]

$$C_i = 0.03895 + 0.48588 \exp\left(-\frac{\mu_{\mathrm{a,bld}}\, r_i}{0.1928}\right) + 0.46803 \exp\left(-\frac{\mu_{\mathrm{a,bld}}\, r_i}{0.91443}\right) \tag{2}$$

We assume blood oxygen saturation of 70% and hematocrit of 40%. By linear interpolation of absorption spectra for oxy- and deoxygenated whole blood at 532 nm as reported by Meinke *et al.*,[15] we obtain $\mu_{\mathrm{a,bld}} = 19.55\ \mathrm{mm}^{-1}$.

The absorption coefficient in the adipose is $\mu_{\mathrm{a,adi}} = 0.075\ \mathrm{mm}^{-1}$.[16]

Table 1. Mean blood vessel radii r_{i} and blood fractions f_{bld},[11] and the resulting absorption coefficient values $\mu_{\mathrm{a},i}$ (2) for the six PWS layers.

i	z (μm)	r_i (mm)	f_i	$\mu_{\mathrm{a},i}$ (mm^{-1})
1	60–260	0.025	0.052	0.383
2	260–460	0.037	0.080	0.436
3	460–660	0.034	0.038	0.247
4	660–860	0.027	0.025	0.204
5	860–1060	0.024	0.020	0.183
6	1060–1560	0.024	0.015	0.151

A wide range of scattering parameters can be found in literature for each human skin constituent. We have tested several combinations of the reported values in MC simulations of both normal (1% blood in dermis) and PWS skin (as Fig. 1, but without the extra vessel). For this study, we have selected the values of μ_{s} and g from recent reports, which resulted in best agreement between the predicted diffuse reflectance at 532 nm and reported experimental values (see

Table 2). The μ_s value for adipose was calculated from the reduced scattering coefficient μ_s' reported by Baskhatov *et al.*[16] and the anisotropy coefficient g as reported by Flock *et al.*[17]

Table 2: Scattering coefficient (μ_s), anisotropy factor (g), and refractive index values (n) used in our Monte Carlo model of optical transport (λ = 532 nm). Values for blood are for hematocrit of 33.2%.

Tissue	μ_s **(mm^{-1})**	g	n
Epidermis	53 [18]	0.770 [18]	1.45 [19]
Dermis	20 [14]	0.770 [18]	1.37 [18]
Blood	69 [15]	0.964 [15]	1.33 [8]
Adipose	6	0.770 [17]	1.34 [16]

The photon launching pattern simulates an incident laser beam with a top-hat profile and diameter of 5 mm, centered above the PWS blood vessel.

2.3 Thermal transport

Temperature field evolution in PWS skin is computed using the two-dimensional heat diffusion equation

$$\rho c_p \frac{\partial T(x,z,t)}{\partial t} = k \nabla^2 T(x,z,t) + S(x,z,t) \tag{3}$$

where k is thermal conductivity, ρ is density, and c_p is specific heat. The heat-source term $S(x,z,t)$ assumes the spatial distribution of energy deposition obtained from MC simulation, and is present only during the 1 ms laser exposure. Heat exchange due to blood perfusion can be neglected during the relatively short time periods considered in this study.

The two-dimensional treatment of heat transport below the laser beam center is sufficient, because – as we demonstrate in the following - heat deposition in this part of VOI is quite homogenous in y direction (i.e., along the vessel axis), therefore heat flow in this direction is negligible.

The thermal constants of skin and blood are the same as used by Jia *et al.*,[8] except the heat capacity of bloodless skin. Temperature dependence of the latter $c_p(T)$ is taken from Xu *et al.*[20] Since temperature in blood can transiently reach boiling conditions, the latent heat of water vaporization is accounted for by augmenting the specific heat term, i.e., $c(T) = c_p + q\, D(T)$, where q is the latent heat of evaporation and $D(T)$ is a normalized Gaussian function.[21] Assuming that strong convection due to nucleation boiling will prevent significant overheating of blood, we center the function $D(T)$ at T_B = 101° C and set its width to ΔT = 1° C. The values for adipose (k = 0.24 W/mK, ρ = 916 kg/m^3, c_p = 3000 J/kgK) are taken from Duck.[22]

At the skin surface ($z = 0$), we apply the convective boundary condition with a heat transfer coefficient H = 5000 W/m^{2}K and outer temperature of –50 °C during the cryogen spurt.[23,24] During the laser pulses and after the cooling/irradiation sequence has ended, we apply a typical natural convection value, H = 10 W/m^{2}K, and ambient temperature (25 °C). Adiabatic boundary condition is applied at $z = \infty$ and $x = \pm\infty$.

Equation (3) is solved using the finite element method within a commercial software package (FEMLAB, COMSOL, CA). The initial skin temperature is set to 35° C.

2.4 Thermal damage model

Thermal damage induced in the modeled tissues is estimated by computing the thermal damage coefficient, Ω, according to the customary Arrhenius model of the coagulation process kinetics. For epidermis and dermis, we use the frequency factor $A = 2.9 \times 10^{37}$ s^{-1} and activation energy E_a = 240 kJ/mol values from Gaylor *et al.*[25] For blood, the values are $A = 7.6 \times 10^{66}$ s^{-1} and E_a = 427 kJ/mol.[26,27]

Calculations of Ω are performed for 100 ms after the last laser pulse to ensure that accumulation of thermal damage has reached a stationary value.

2.5 Simulation study protocol: Sequential irradiation of a PWS vessel with intermittent cryogen spray cooling

As a demonstration example, we consider sequential irradiation of a model PWS vessel with intermittent cryogen spray (CS) cooling, in comparison with the customary approach, using a single laser pulse (LP) preceded by CS cooling. The sequence consists of the initial 50 ms cryogen spurt followed by 1 ms LP, followed in turn by four pairs of CS (duration: 100 ms) and LP.

We simulate both treatment approaches and calculate Ω at the epidermal-dermal junction (z = 60 μm) at gradually increasing radiant exposures (in increments of 0.1 J/cm^2). In this manner, we determine the respective maximal radiant exposure values, H_{epi}, where no epidermal damage is generated ($\Omega_{epi} \leq 1$). In order to mimic a realistic treatment scenario, the following examples are computed at 80% of the epidermal threshold values (H_{epi}) for each irradiation regime.

3. RESULTS

3.1 Diffuse reflectance

Using the presented MC optical model, we first compute total reflectance (a sum of diffuse and specular reflection components) at 532 nm for healthy skin (1% blood distributed evenly throughout the dermis). For various skin types, we use epidermal absorption coefficient values computed from experimental results at 694 nm by Svaasand *et al.*[9] using the wavelength dependence relations by Jacques.[10]

In this manner, we get $\mu_{a,epi}$ = 0.81 mm^{-1} (f_{mel} = 3.5%) for fair Caucasian skin. By using the remaining absorption and scattering coefficient from Tables 1 and 2, respectively, this yields a reflectance value of R = 0.31. This result matches the value reported by Randeberg *et al.*[28] for North European skin, and falls within the range of values measured by Svaasand *et al.*[9] in the same skin type (R = 0.25–0.33).

For heavily pigmented Middle Eastern and Asian skin, the same procedure yields $\mu_{a,epi}$ = 2.33 mm^{-1} (f_{mel} = 4.1%), a little higher than the value used in the rest of this study. The resulting reflectance value from our model is R = 0.19, which matches well with the values reported for Asian skin by Svaasand *et al.*[9] (R = 0.19) and Randeberg *et al.*[28] (R = 0.20).

3.2 Laser energy deposition

Figure 2 shows spatial distribution of deposited laser energy as obtained by our MC simulation of PWS in moderately pigmented Middle Eastern or Asian skin upon irradiation with a 5 mm diameter hat-top laser beam at λ = 532 nm and radiant exposure H = 4.6 J/cm^2. In the central plane perpendicular to the vessel axis (y = 0.5 mm; Fig. 2a), the energy

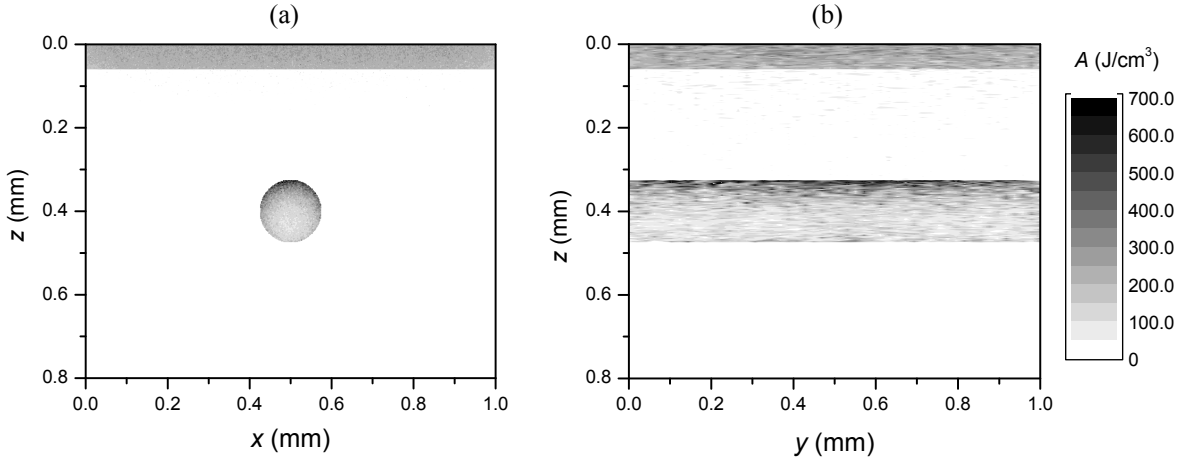

Figure 2. Cross-sectional maps of the energy energy deposited in PWS lesion with a model blood vessel (d = 150 μm, z_0 = 400 μm) upon irradiation with a 5 mm diameter hat-top laser beam at λ = 532 nm and radiant exposure H = 4.6 J/cm^2; (a) – in the central plane (y = 0.5 mm) perpendicular to the vessel axis; (b) – along (through) the vessel axis.

deposition within the vessel is non-uniform with the largest values near the top vessel boundary. Figure 2b presents the energy distribution in the vertical plane through the vessel axis.

Figure 3a presents the depth profile of energy deposition through the vessel axis ($x = y = 0.5$ mm) from the data in Fig. 2. The result reveals the subsurface peak of light fluence in the epidermis and the "shadow" immediately underneath the model vessel, which occurs despite the strong scattering of light in the dermis. Horizontal energy deposition profile through the vessel axis from the same data ($y = z = 0.5$ mm; Fig. 3b) shows the similar (albeit much less pronounced) reduction of light fluence in the vicinity of the model vessel in lateral direction.

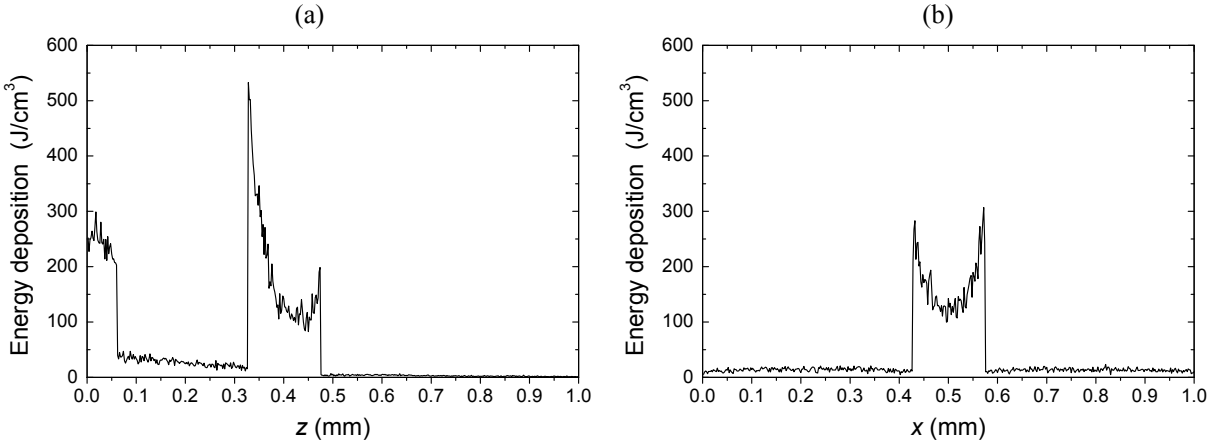

Figure 3. Energy deposition profiles from the result in figure 2: (a) – vertical direction, through vessel axis ($x = y = 0.5$ mm); (b) – horizontal, through the vessel axis.

Figure 4 presents the corresponding energy deposition profiles in the direction parallel to the vessel axis. Energy deposition in the epidermis near the surface (Fig. 4a, lighter line) is nearly constant across the entire VOI, and not significantly different from that near the border with dermis ($z = 60$ μm; heavier line). Energy deposition along at the top of the PWS vessel (Fig. 4b, lighter line) is also rather constant, except the 0.1–0.2 mm wide part near the VOI border. Energy deposition along at the vessel axis (heavier line) and bottom of the lumen (short dash) are again constant and very similar, but significantly lower as compared to the vessel top, or even the epidermis (Fig. 4a).

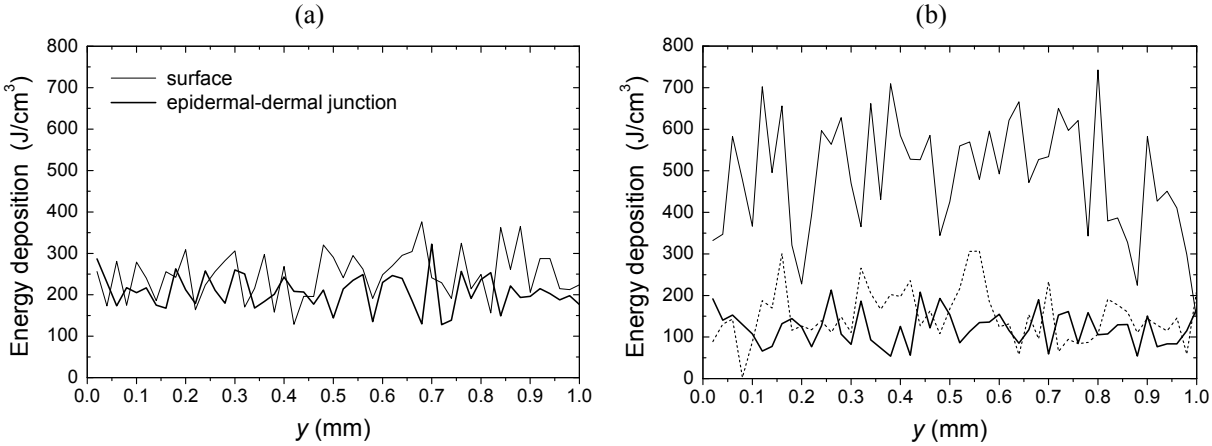

Figure 4. Energy deposition profiles in the direction parallel to the vessel axis: (a) – in the epidermis, near the surface and at the border with dermis ($z = 60$ μm; see the legend); (b) – at the top (lighter line), center (heavier line) and bottom of the vessel lumen (short dash).

3.3 Temperature evolution and distribution

In Figure 5 we present temperature evolution at the top, center, and bottom of the model PWS vessel (diameter d = 150 μm, axis depth z_0 = 400 μm). For the case of single laser pulse (n = 1; left panel), temperature at the top of the vessel reaches 91.5 °C (thin solid line) at H = 4.6 J/cm^2 (i.e., 20% below the epidermal damage threshold, H_{epi}), as compared to only 55.4 °C at the vessel bottom (dashed line).

For the sequence of five laser pulses with intermittent cryogen spray cooling at repetition rate of 10 Hz and radiant exposure per pulse H = 4.4 J/cm^2 (also equal to 80% of the respective H_{epi}; right panel), temperature at the vessel center peaks at 92.1 °C (heavy line), which is much higher than after the single laser pulse (75.7 °C; left panel). Hence, heat accumulation within the PWS vessel upon application of the CS cooling/ LP heating sequence clearly results in significantly higher and much more uniform temperature rise across the entire vessel lumen, as compared to the customary single-pulse approach.

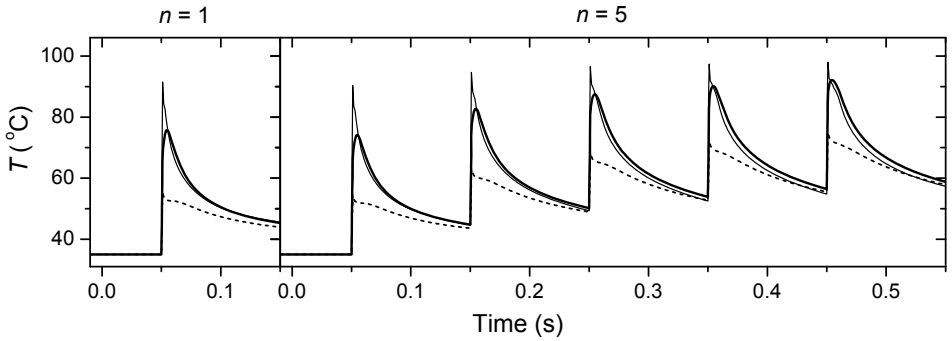

Figure 5. Temperature evolution in the model PWS blood vessel for irradiation with a single laser pulse (n = 1; left panel) and a sequence of five laser pulses with intermittent cryogen spray cooling (right). Temperatures at the top (thin line), center (heavy line), and bottom (short dash) of the vessel lumen are presented. Radiant exposure per pulse equals 80% of the epidermal damage threshold, i.e., H = 4.6 J/cm^2 and 4.4 J/cm^2 for n = 1 and n = 5, respectively.

Figure 6 shows temperature evolution at the epidermal-dermal junction for the same two examples as above (Fig. 5). In either example, radiant exposure per pulse equals 80% of the epidermal damage threshold, H_{epi}. The initial 50 ms CS reduces temperature at the epidermal-dermal junction to 10 °C. Thereafter, the single laser pulse heats the epidermis to the maximum temperature of 47.0 °C (left panel). In contrast, the maximal temperature reached during the sequential CS cooling and laser heating is 45.6 °C, and no accumulation of heat in the epidermis is observed.

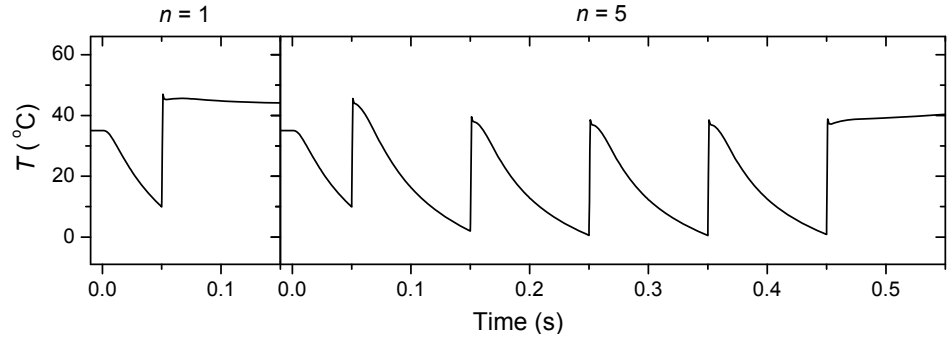

Figure 6. Temperature evolution in the epidermis near the epidermal-dermal junction (z = 60 μm) under the same irradiation conditions as in figure 5: a 50 ms cryogen spurt followed by 1 ms laser pulse (left panel) and a sequence of 5 laser pulses with intermittent cryogen spray cooling (right).

Figure 7a presents temperature distribution in the central cross-sectional plane of the model PWS geometry, at the end of the single pulse irradiation preceded by 50 ms CS cooling. Temperature at the bottom of the vessel lumen is 53 °C, significantly less than at the top (91.7 °C). In contrast, temperatures at the same points in the vessel after irradiation with the sequence of 5 laser pulses at f = 10 Hz with intermittent CSC amount to 72.6 and 97.9 °C, respectively, while the epidermal temperature rise is clearly significantly smaller as compared to the former case (Fig. 7b).

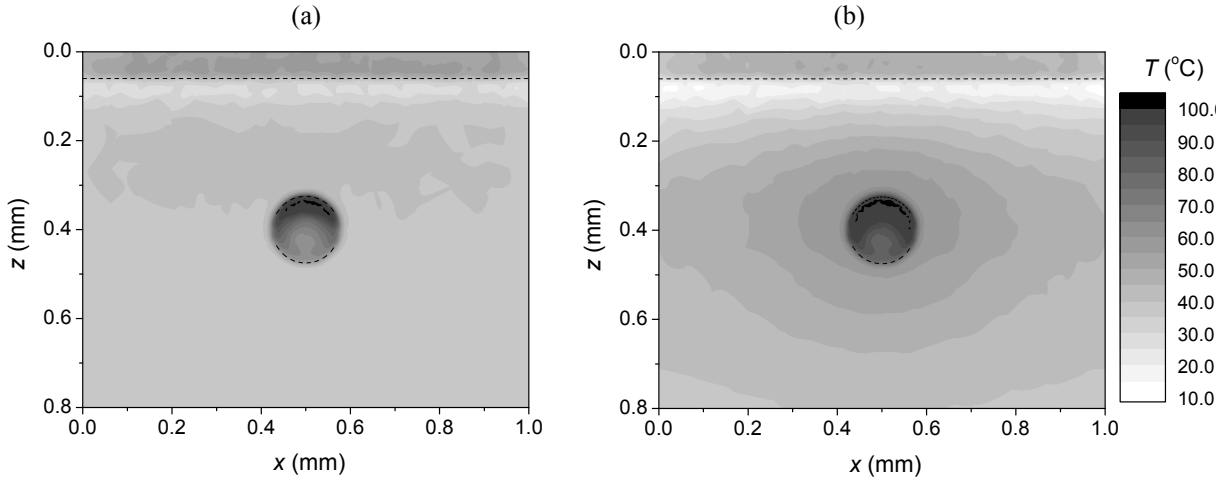

Figure 7. Temperature field in the central plane of the model PWS geometry (y = 0.5 mm) immediately after irradiation with: (**a**) a 1 ms laser pulse at 532 nm; (**b**) a sequence of 5 laser pulses with intermittent CSC at f = 10 Hz. The respective radiant exposure values are the same as in figures 6a and 6b.

This is even more apparent in Fig. 8, showing the vertical temperature profiles through the vessel center ($x = y$ = 0.5 mm) for the same examples – single-pulse (dashed line) and sequential CS/LP treatment of the simulated PWS lesion (solid line).

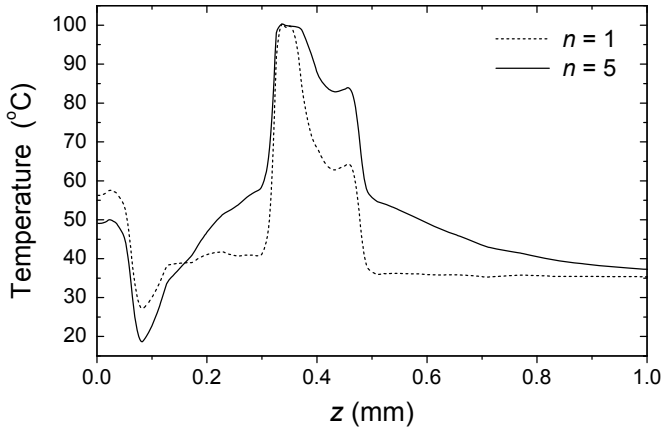

Figure 8. Vertical temperature profiles through the vessel center ($x = y$ = 0.5 mm) from the data in figure 7a (dashed line) and figure 7b (solid line).

3.4 Coagulation maps

The extent of tissue coagulation resulting from both treatment approaches is illustrated in Figure 9 by presenting the cross-sectional distributions of the damage parameter Ω. Coagulation of blood and dermis is indicated by darker gray shade ($\Omega \geq 1$), while white to light gray areas represent healthy and partly compromised tissue, respectively. The model PWS vessel is only partly coagulated by the single laser pulse (Figure 9a), but the sequential approach results in complete coagulation of the vessel lumen (Figure 9b). The CS/LP sequence also causes some thermal damage in perivascular dermis, extending approximately 20 μm from the edge of the vessel lumen. Since the radiant exposure in either case is 20% lower than the corresponding epidermal damage threshold, no thermal damage to the epidermis (above the dashed line) is evident.

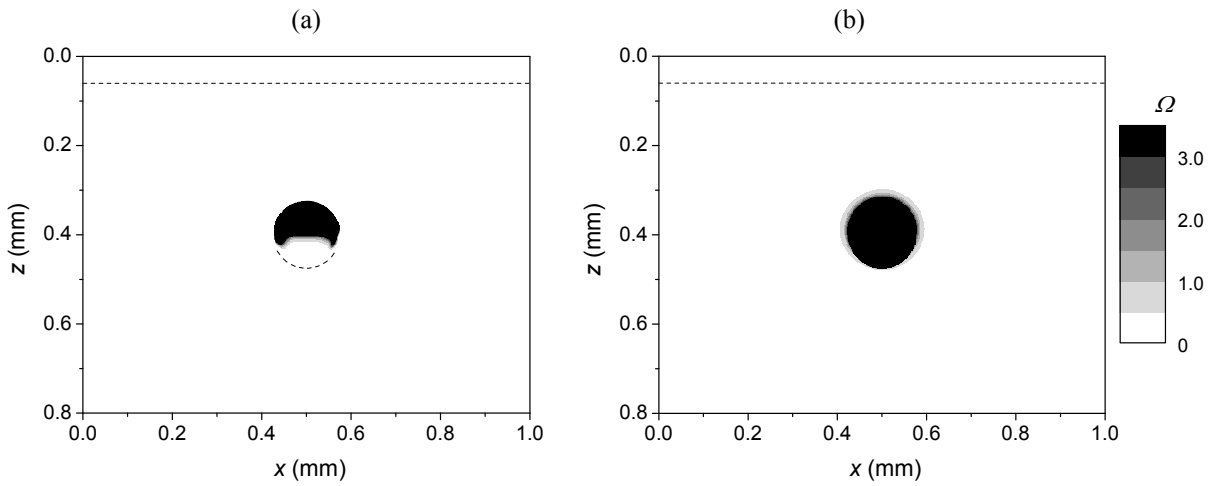

Figure 9. Cross-sectional maps of the coagulation parameter Ω: (**a**) - after irradiation with 1 ms laser pulse after CS cooling; (**b**) – after a sequence of 5 laser pulses at 10 Hz with intermittent CS. Radiant exposure in either example is 20% below the epidermal damage threshold, i.e., 4.6 J/cm^2 and 4.4 J/cm^2 per pulse for (a) and (b), respectively.

4. CONCLUSIONS

Our three-dimensional MC optical model with augmented approach to the boundary problem allows treatment of small volumes of irradiated skin with inclusions of arbitrary shape. Using the updated values of optical properties of involved tissues and respective coefficients of the Arrhenius model of tissue coagulation kinetics we obtain realistic values of diffuse reflectance in normal skin, as well as thresholds for epidermal thermal damage and therapeutic effect in PWS laser treatment.

The example simulation of PWS treatment indicates that specific sequences of intermittent cryogen spray cooling and sequential pulsed laser irradiation may offer higher efficacy and safety as compared to the customary single-pulse approach, especially in patients with larger and deeper PWS blood vessels and skin types. In a follow-up study, based on the same numerical model, we have identified the specific parameters of sequential CS cooling and laser irradiation that allow optimal photocoagulation of PWS blood vessels with minimal risk of epidermal thermal damage across a wide range of PWS structures and skin types.[29]

REFERENCES

[1] Wang, L., Jacques, S. L., Zheng, L., "MCML - Monte Carlo modeling of light transport in multi-layered tissues," Comp. Methods Prog. Biomed. 47(2), 131-146 (1995).

[2] Anderson, R. R., Parrish J. A., "Selective photothermolysis: Precise microsurgery by a selective absorption of pulsed radiation," Science 220, 524-527 (1983).

[3] Nelson, J. S., Milner, T. E., Anvari, B., Tanenbaum, B. S., Kimel, S., Svaasand, L. O., Jacques, S. L., "Dynamic epidermal cooling during pulsed laser treatment of port-wine stain," Arch. Dermatol. 131, 695–700 (1995).

[4] van der Horst, C. M. A. M., Koster, P. H. L., de Borgie, C. A. J. M., Bossuyt, P. M. M., van Gemert, M. J. C., "Effect of the timing of treatment of port-wine stains with the flash-lamp-pumped pulsed dye-laser," New Eng. J. Med. 338, 1028-1033 (1998).

[5] Lanigan, S. W., "Port-wine stains unresponsive to pulsed dye laser: explanations and solutions," Br. J. Dermatol. 139, 173-177 (1998).

[6] Lucassen, G. W., Verkruysse, W., Keijzer, M., van Gemert, M. J. C., "Light distributions in a port wine stain model containing multiple cylindrical and curved blood vessels," Laser Surg. Med. 18, 345-357 (1996).

[7] Hohenleutner, U., Hilbert, M., Wlotzke, U., Landthaler, M., "Epidermal damage and limited coagulation depth with the flashlamp-pumped pulsed dye laser: A histochemical study," J. Invest. Dermatol. 104, 798–802 (1995).

[8] Jia, W., Choi, B., Franco, W., Lotfi, J., Majaron, B., Aguilar, G., Nelson, J. S., "Treatment of cutaneous vascular lesions using multiple-intermittent cryogen spurts and two-wavelength laser pulses: Numerical and animal studies," Laser Surg. Med. 39(6), 494–503 (2007).
[9] Svaasand, L. O., Norvang, L. T., Fiskerstrand, E. J., Stopps E. K. S., Berns, M. W., Nelson, J. S., "Tissue parameters determining the visual appearance of normal skin and port-wine stains," Laser Med. Sci. 10, 55–65 (1995).
[10] http://omlc.ogi.edu/spectra/melanin/mua.html
[11] Barsky, S. H., Rosen, S., Geer, D. E., Noe, J. M., "The nature and evolution of port wine stains: A computer-assisted study," J. Invest. Dermatol. 74, 154–157 (1980).
[12] Ross, E. V., Domankevitz, Y., "Laser treatment of leg veins: physical mechanisms and theoretical considerations," Laser Surg. Med. 36(2), 105–116 (2005).
[13] Verkruysse, W., Lucassen, G. W., de Boer, J. F., Smithies, D. J., Nelson, J. S., van Gemert, M. J. C., "Modeling light distributions of homogenous versus discrete absorbers in light irradiated turbid media," Phys. Med. Biol. 42, 51–65 (1997).
[14] Choi, B., Majaron, B., Nelson, J. S., "Computational model to evaluate port wine stain depth profiling using pulsed photothermal radiometry," J. Biomed. Opt. 9(2), 299–307 (2004).
[15] Meinke, M., Müller, G., Helfmann, J., Friebel, M., "Optical properties of platelets and blood plasma and their influence on the optical behavior of whole blood in the visible to near infrared wavelength range," J. Biomed. Opt. 12, 014024-1–014024-9 (2007).
[16] Bashkatov, A. N., Genina, E. A., Kochubey, V. I., Tuchin, V. V., "Optical properties of the subcutaneous adipose tissue in the spectral range 400–2500 nm," Opt. Spect. 99, 836–842 (2005).
[17] Flock, S. T., Wilson, B. C., Patterson, M. S., "Total attenuation coefficients and scattering phase functions at tissues and phantom materials at 633 nm," Med. Phys. 14, 835–841 (1987).
[18] Barton, J. K., Pfefer, T. J., Welch, A. J., "Optical Monte Carlo modeling of a true port wine stain anatomy," Opt. Express 2, 391–296 (1998).
[19] Ding, H., Lu, J. Q., Wooden, W. A., Kragel, P. J., Hu, X. H., "Refractive indices of human skin tissues at eight wavelengths and estimated dispersion relations between 300 and 1600 nm," Phys. Med. Biol. 51, 1479–1489 (2006).
[20] Xu, F., Seffen, A., Lu, T. J., "Temperature-dependent mechanical behaviors of skin tissue," IAENG Int. J. Comp. Sci.35, 1–13 (2008).
[21] Shafirstein, G., Baumler W., Lapidoth, M., Ferguson, S., North, P. E., Waner, M., "A new mathematical approach to the diffusion approximation theory for selective photothermolysis modeling and its implication in laser treatment of port-wine stains ," Laser Med. Sci. 34, 335–47 (2006).
[22] Duck, F. A., [Physical properties of tissue], Academic Press, London (1990).
[23] Majaron, B., Svaasand, L. O., Aguilar, G., Nelson, J. S., "Intermittent cryogen spray cooling for optimal heat extraction during dermatologic laser treatment," Phys. Med. Biol. 47(18), 3275–3288 (2002).
[24] Svaasand, L. O., Randeberg, L. L., Aguilar, G., Majaron, B., Kimel, S., Lavernia, E. J., Nelson, J. S., "Cooling efficiency of cryogen spray during laser therapy of skin," Laser Surg. Med. 32(2), 137-142 (2003).
[25] Gaylor, D. C. [Physical mechanism of cellular injury in electrical trauma], Ph.D. thesis, Massachusetts Institute of Technology, Cambridge, MA (1989).
[26] Nilsson, A. M. K., Lucassen, G. W., Verkruysse, W., Andersson, E. S., van Gemert, M. J. C., "Changes in optical properties of human whole blood in vitro due to slow heating," Photochem. Photobiol. 65, 366–373 (1997).
[27] Barton J. K., Rollins A., Yazdanfar S., Pfefer T. J., Westphal V., Izatt J. A., "Photothermal coagulation of blood vessels: a comparison of high-speed optical coherence tomography and numerical modelling," Phys. Med. Biol. 46, 1665–78 (2001).
[28] Randeberg, L. L., Haugen, O. A., Haaverstad, R., Svaasand, L.O., "A novel approach to age determination of traumatic injuries by reflectance spectroscopy," Laser Med. Sci. 38, 277–89 (2006).
[29] Milanič, M., Jia, W., Nelson, J. S., Majaron, B., "Numerical optimization of sequential cryogen spray cooling and laser irradiation for improved therapy of port wine stain," Laser Surg. Med. (submitted).